Arabian Journal of Chemistry (2022) **15**, 103586

King Saud University

Arabian Journal of Chemistry

www.ksu.edu.sa
www.sciencedirect.com

ORIGINAL ARTICLE

Solvent free synthesis, characterization, DFT, cyclic voltammetry and biological assay of Cu(II), Hg(II) and UO_2(II) – Schiff base complexes

Samah J. Almehmadi [a], Arwa Alharbi [b], Matokah M. Abualnaja [b], Kholood Alkhamis [c], Mona Alhasani [b], Shams H. Abdel-Hafez [d], Rania Zaky [e], Nashwa M. El-Metwaly [b,e,*]

[a] *Department of Laboratory Medicine, Faculty of Applied Medical Sciences, Umm Al Qura University, Makkah 21955, Saudi Arabia*
[b] *Department of Chemistry, Faculty of Applied Science, Umm Al Qura University, Makkah, Saudi Arabia*
[c] *Department of Chemistry, College of Science, University of Tabuk, Tabuk, Saudi Arabia*
[d] *Department of Chemistry, College of Science, Taif University, P.O. Box 11099, Taif 21944, Saudi Arabi*
[e] *Department of Chemistry, Faculty of Science, Mansoura University, Mansoura, Egypt*

Received 30 September 2021; accepted 21 November 2021
Available online 25 November 2021

KEYWORDS

Schiff base-complexes;
Solvent free synthesis;
DFT;
Cyclic voltammetry;
Biological activity

Abstract A series of metal ion complexes was prepared in solid state from Cu(II), Hg(II) and UO_2(II) ions with 3-oxo-3-(2-(2-oxoindolin-3-ylidene)hydrazineyl)-N-phenylpropanamide (H_3L) ligand through solvent free synthesis methodology. The chemical formulae of the new compounds were estimated according to variable spectral and analytical investigations. The ligand exhibited a neutral or mononegative tetradentate mode of coordination towards the central ions inside the octahedral arrangement that proposed for the three complexes. The DFT/B3LYP method was applied under different basis sets (6-31G*or SDD) to optimize the structures of new compounds except the UO_2(II) complex. The computational data were investigated to verify the binding mode that suggested spectrally. Moreover, studies in solution regarding Cu(II) ion *via* cyclic voltammetry were performed in absence or presence of H_3L, to realize the significant effect of complex formation on the electrochemical manners of copper. The shifts in the potential peaks accompanied by the changes in the values of parameters correspond to kinetic and thermodynamic. Also, the solvation

* Corresponding author.
E-mail addresses: sjamehmadi@uqu.edu.sa (S.J. Almehmadi), awharbi@uqu.edu.sa (A. Alharbi), mmabualnaja@uqu.edu.sa (M.M. Abualnaja), kalkhams@ut.edu.sa (K. Alkhamis), mamhasani@uqu.edu.sa (M. Alhasani), s.abdelhafez@tu.edu.sa (S.H. Abdel-Hafez), rania.zky@yahoo.com (R. Zaky), n_elmetwaly00@yahoo.com (N.M. El-Metwaly).
Peer review under responsibility of King Saud University.

Production and hosting by Elsevier

https://doi.org/10.1016/j.arabjc.2021.103586

and kinetic characteristics for the cathodic and anodic potential of Cu(II) ion in absence or presence of H_3L at different scan rates, were estimated. Finally, the ligand and copper ion exhibited high affinity towards complexation in solution. Furthermore, the activity of the new compounds towards inhibiting microbes was studied against *Staphylococcus aureus (G+)* and *Escherichia coli* (*G*-) bacteria as well as *Candida albicans* (fungus) by determining the inhibition zone diameter. Also, both the antioxidant and cytotoxic activity of the isolated compounds were evaluated. Commonly, a remarkable antimicrobial and anticancer activity was appeared with UO_2(II) complex and the ligand. While, the antioxidant activity of all compounds appeared lower.

1. Introduction

Schiff base ligands are a popular family of ligands due to their many useful properties, including their ability to be modified by adding different donor groups that lead to high flexibility (Abu-Dief et al., 2021; Atkins et al., 1996). Functional diversity conducts to variable coordination numbers which provided by these easily available ligands that coordinating to different metals utilized for complex production. Imines have encouraged scientists in the domains of magnetochemistry, bioinorganic chemistry, analytical chemistry, encapsulation, catalysis, separation, and transport science to create metal complexes due to their numerous advantages. Such ligands have good biological properties, and as a result, they've been used in a variety of catalytic, anticancer, and antimicrobial researches. The main demand in the pharmaceutical industry is for new pharmacological agents with diverse mechanisms and low side effects, especially for the treatment of infections and malignancies. As a result, new sensitizing agents that can selectively boost the cytotoxicity of chemotherapeutic medicines to cancer cells must be developed (Sönmez et al., 2010).

4-aminoantipyrine ligand was utilized in a green approach to prepare variety of bivalent metal ion complexes that exhibited excellent interaction with DNA (Sönmez et al., 2010). The complexes of Cu(II)-Schiff bases were fully characterized and exhibited higher anti-inflammatory action (Katouah et al., 2020a,b). Macrocyclic Ni(II) and Co(II) complexes have been synthesized and successfully employed as CO_2-reduction catalysts (Katouah et al., 2019). The ligand synthesized from propane hydrazide was used to isolate divalent metal ion complexes by a green method and the majority of the complexes displaying biological activity (Fisher et al., 1980; Al-Hazmi et al., 2017). The salicylaldehyde derivative was utilized to isolate Schiff base ligand, which used to obtain Cu(II) and Ni(II) complexes that fully characterized (Alkhatib et al., 2020). Green synthesis of Ni(II), Pd(II) and Cu(II) complexes that derived from Schiff base derivative, were tested for antibacterial, antioxidant, and anticancer activities, and the majority of them showed good findings (Morgan et al., 2017). A series of Co(II), Ni(II) and Cu(II) complexes was derived from a Schiff base derivative and described before being utilized as a catalyst in hydrogen peroxide oxidation of cyclohexane (Shah et al., 2020; Tamami et al., 2015). Antitumor action was observed for new nickel, copper and cobalt complexes that derived from hydrazide ligand (Antony et al., 2013). The electrochemical features of nano-sized Cu(II) complex were investigated (Al-Qahtani et al 2012; Munshi et al., 2021). Also, a green synthesis of copper complex yielded from Schiff base derivative was achieved and its potentiometric parameters were estimated (Al-Qahtani et al 2012; Munshi et al., 2021).

Interestingly to note that, the chemical composition produced numerous environmental issues, therefore researchers tried to make their composition as risk-free as possible. As a result, preparation without the use of a solvent as a green protocol is a goal that has already been achieved in a number of publications employing the ball milling technique (Sönmez et al., 2010; Fisher et al., 1980; Al-Hazmi et al., 2017). The reactants (metal salt and ligand) are perfectly grinding in a ball mill without solvent, resulting in a simple reaction that is first visible as discoloration away from the starting compounds. After washing the solid complexes numerous times with a suitable solvent, the purity of the complexes was confirmed (Morgan et al., 2017; Al-Qahtani et al 2012; Munshi et al., 2021).

We planned to make a new Schiff base derivative based on all of the studies described and in continuation of our work (Alzahrani et al 2020; Katouah et al., 2020a,b; Abumelha et al., 2020). This derivate was characterized and then utilized to synthesize its Cu(II), Hg(II) and UO_2(II) complexes in solvent free. The geometry of each complex was suggested based on analytical and spectral studies, also confirmed *via* DFT/B3LYP method, which utilized for structural optimization. In addition, some kinetics and solvation parameters were estimated from cyclic voltammograms of Cu(II) complex (i.e.). A comprehensive biological study was conducted to evaluate the behavior of new compounds towards microbes, free-radical sources and carcinoma cell line.

2. Experimental

2.1. Chemicals

The compounds utilized to prepare Schiff base ligand and its metal ion complexes were 3-hydrazineyl-3-oxo-N-phenylpropanamide, isatin, $Cu(OAc)_2{\cdot}2H_2O$(98%), $UO_2(OAc)_2{\cdot}2H_2O$ (98%) and $HgCl_2$ (99%). Absolute ethanol (EtOH) and dimethyl sulfoxide (DMSO) solvents employed either for the ligand synthesis or to dissolve the complexes for analytical purposes, were spectroscopic in nature. The reagents of 2, 2′-azinobis-(3-ethylbenzthiazoline-6-sulphonic acid)(ABTS) and L-ascorbic acid which utilized for biological tests were provided by Sigma-Aldrich. Also, HepG2 cell line was donated by ATCC's company which holding biological products and vaccines (VACSERA) for cytotoxic assay. Notice: all these

reagents were purchased from Sigma-Aldrich were BDH in nature.

2.2. Synthesis of the ligand and its metal complexes

In 50 mL absolute ethanol, equal moles (1:1) of 3-hydrazineyl-3-oxo-N-phenylpropanamide (0.01 mol; 1.93 g) and isatin (0.01 mol; 1.47 g) were mixed to isolate the ligand. For 3 h, the reaction mixture was maintained at 80 °C during reflux. Then after that the mixture was concentrated to reach to the half volume, and set aside to cool. Filtration was used to extract the product, which was then recrystallized from EtOH and dried in vacuum desiccators over anhydrous $CaCl_2$. The ligand isolated was (*E*)-3-oxo-*N'*-(2-oxoindolin-3ylidene)-3-(p henylamino) propane hydrazide and abbreviated H_3L according to existence of three labile hydrogen atoms that may be ionization easily (Scheme 1). Equi-molar ratios from the ligand (3 mmol, 0.966 g) and each of $Cu(OAc)_2{\cdot}2H_2O$ (3 mmol, 0.653 g), $UO_2(OAc)_2{\cdot}2H_2O$ (3 mmol, 1.272 g) or $HgCl_2$ (3 mmol, 0.815 g) salt were grinded without unpleasant solvent except few drops of water to aid grinding, only. The time taken to prepare the Cu(II) complex is smaller (5 min) than that used with the other complexes (15 min). The acidic smell was noticed during the synthesis of Hg(II) and UO_2(II) complexes, which denotes the deprotonation of the ligand due to high heat generated during vigorous grinding inside ball milling. The first indicator of the reaction is the color of the solid resulted, which is entirely different from the reactants and thin layer chromatography(TLC) test confirms the product purity (Antony et al., 2013; Al-Qahtani et al 2012; Munshi et al., 2021;). Notice: Table 1, lists some physical and analytical properties of the new compounds.

2.3. Instrumentation

For clarity, the approaches employed for the analyses are depicted as images in the supporting materials file (Scheme S1). Moreover, each device's description has been given below, while the implementation conditions will be reported individually in the discussion section. Complexometric titration was used to assess the metal content (without uranium), while the gravimetric analysis was used to determine the chloride content (Vogel et al., 1989). On the other side, after complete combustion of weighed sample in open air and then in oven at 800 °C until the organic compound was completely

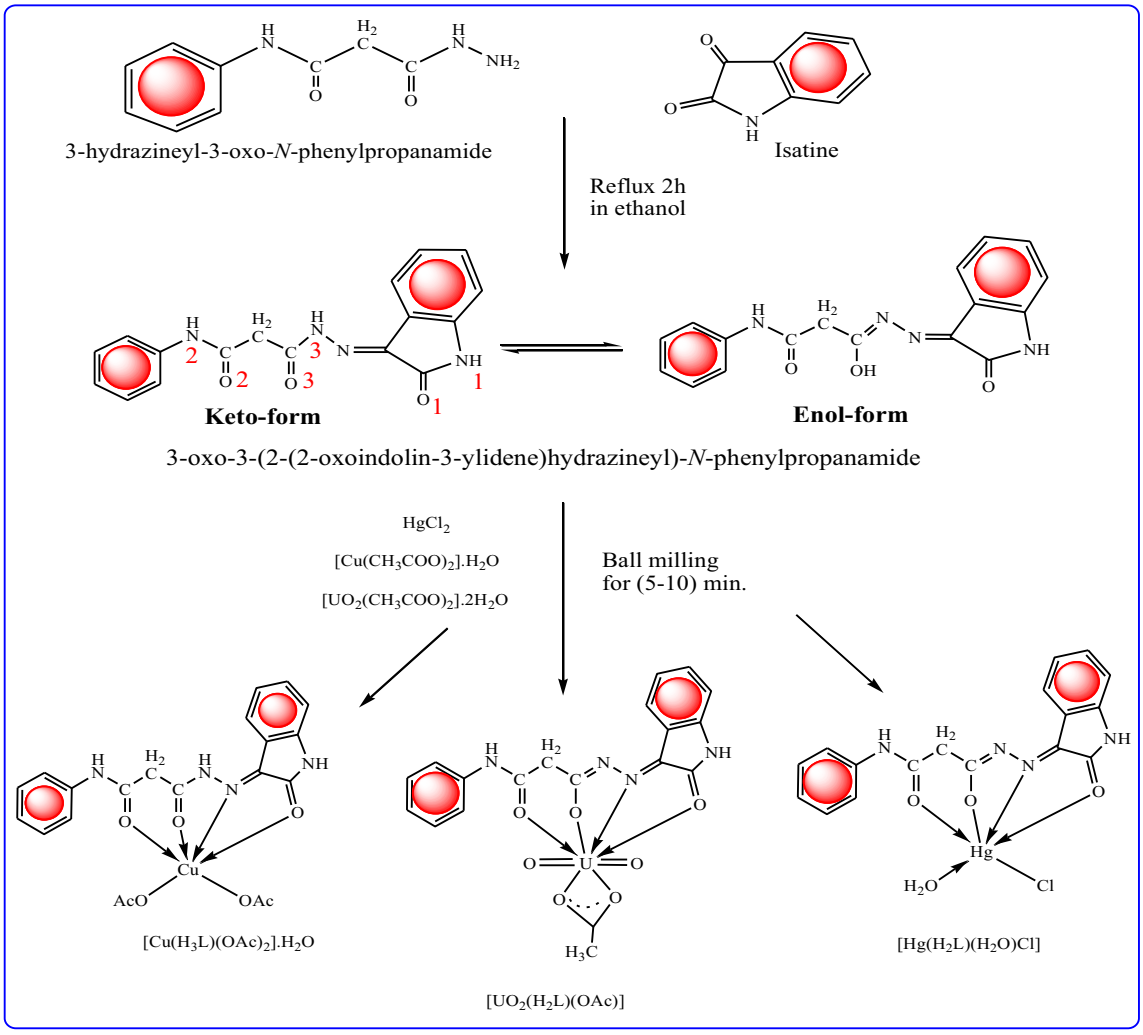

Scheme 1 Synthesis outlines for the ligand and its metal complexes.

Table 1 Analytical and physical data of H_3L and the new complexes.

Compound	Empirical Formula (Molecular mass) Calcd	Color	MP (°C)	Yield (%)	%Found (Calcd.)				
					C	H	M	Cl	Λ_m*
H_3L	$C_{17}H_{14}N_4O_3$ 322.320	Yellow	260	85	63.41 (63.35)	4.40 (4.38)	–	–	–
$[UO_2(H_2L)(OAc)]$	$UC_{19}H_{15}N_4O_7$ 649.436	Reddish-brown	> 300	99	35.16 (35.13)	2.29 (2.33)	36.60 (36.65)	–	4
$[Hg(H_2L)(H_2O)Cl]$	$HgC_{17}H_{14}N_4O_4Cl$ 574.442	Yellow	290	99	35.60 (35.54)	2.43 (2.46)	34.88 (34.91)	6.14 (6.18)	7
$[Cu(H_3L)(OAc)_2].H_2O$	$CuC_{21}H_{24}N_4O_8$ 520.885	Brown	> 300	98	48.39 (48.42)	4.70 (4.64)	12.22 (12.19)	–	9

* In DMSO ($ohm^{-1}cm^2\ mol^{-1}$)

evaporated, the percentage of uranium was calculated from the residual part weight (U_3O_8).

2.4. Geometry optimization

Gaussian 09 (Frisch et al., 2009) was deemed the best molecular modeling application that was used to verify practically accepted structures for the substances under investigation. The DFT/B3LYP method that implemented the valent electron basis set (SDD) (Lee et al., 1988; Li et al., 2016) and the polarized function within valence double-zeta basis set (6-31G*), was applied for optimization [Li et al., 2016]. The SDD was identified as the best core potential basis set for the Hg(II) complex [Li et al., 2016], while 6-31G* was sufficient for organic ligands and the other complexes, with 6-d-functions added as polarized functions to 6-31G set. The DFT was done at B3LYP level (Becke et al 1993) to investigate both states of ground and excited attributes utilizing Integral Equation Formalism Variant (IEF-PCM) with a polarizable continuum model. Using Gauss-View and Gauss-Sum 2.2 programs, all quantum data was extracted from two exported computational files, as well as the third that extracted after formulation for chk file on Gauss-prog (fchk) (Dennington et al., 2007). Finally, we were unable to apply an appropriate basis set for structural optimization of UO_2(II) complex since we couldn't discover its computational properties.

2.5. Cyclic voltammetry

This electro-analytical technique was applied for $CuCl_2$ in solution either in absence or in presence of the ligand. The cell used is a small beaker containing 0.L M KCl (30 mL) as a supporting electrolyte. A reference electrode, Ag/AgCl/KCl (saturated), the glassy carbon working electrode (GCWE), and platinum wire as an auxiliary electrode were used. These electrodes were dipped in KCl solution and connected with potentiostat.

2.6. Biological activity

2.6.1. Antimicrobial and antioxidant assays

The antibacterial activity of the novel compounds was assessed using agar-well diffusion technique (Hawkey et al., 1994). In supporting materials, the procedure was described in depth (Scheme S1).

The success of new compounds to scavenge free radicals produced *via* 2, 2′-azinobis-(3-ethylbenz thiazoline-6-sulphonic acid)(ABTS) compound, reflects their antioxidant efficiency which could being evaluated. This method has been effectively utilized to test the materials' ability to combat free radicals (Re et al., 1999). An outline of the procedure is presented in Scheme S3 for clarity. The mixtures were stirred, centrifuged, and filtered immediately. Initial absorbance ($A_{control}$) measurements at λ = 734 nm were used to measure the strength of the green–blue color developed. As a result, after dissolving 2 mM of each examined chemical in 50L MeOH/buffer (1:1; v/v), the absorbance (A_{test}) was calculated. The absorbance value was utilized to calculate the actual color intensity decay, which was then used as antioxidant activity indicator. $[A_{(control)}\text{-}A_{(test)}/A_{(control)}]\times$ 100, was the relation used to calculate the inhibition percentage. The positive control used was the vitamin C and the ascorbic acid was the standard drug utilized. The implemented blank was the buffer from methanol and phosphate (1:1) solution which is free of ABTS and then the substance being evaluated.

2.6.2. MTT cytotoxicity assay

3-(4,5-dimethylthiazol-2-yl)-2,5-diphenyl tetrazolium bromide (MTT) approach was applied to examine cancer cell (HepG2) proliferation (Mosmann et al., 1983; Mohamed et al 2017) under the influence of new compounds. The reference drug was 5-fluorouracil which used for comparison with the tested compounds, and the experimental phases were presented elaborately in Scheme S4.

3. Results and discussion

3.1. Analytical features

To explain their chemical formulae, the ligand (H_3L) and its corresponding Cu(II), Hg(II), and UO_2(II) complexes, were physically and chemically studied (Table 1). The new complexes appeared with high stability, non-moisture absorbent, and high melting points. The non-conducting property of all complexes was assumed based on the conductivity of 10^{-3}M (Λ_m, $\Omega^{-1}cm^2mol^{-1}$) that determined in DMSO solvent (Geary et al 1971). All complexes were recommended in equal molar ratios (1 M:1L) based on elemental analysis, which was later confirmed by EDX analysis (part 3.5).

3.2. Spectral analysis for Schiff base ligand

The most notable infrared bands of H_3L and its complexes are mentioned in Table 2. The bands found in the IR spectrum of H_3L (Fig. S1) at 1742, 1686, and 1662 cm^{-1} are attributing to υ(C = O)$_1$, υ(C = O)$_2$ and υ(C = O)$_3$ (Alharbi et al., 2021) vibrations, respectively. A weak band at 1078 cm^{-1} is attributing to υ(N-N) vibration. Sequentially, the vibrations of υ(NH)$_1$, υ(NH)$_2$, υ(NH)$_3$ and υ(CH)$_{aromatic}$, were appeared at 3200, 3303, 3259, and 3009 cm^{-1} (Alharbi et al., 2021; Nakamoto, 1970). The band at 3451 cm^{-1} may assign to υ(C-OH), which produced *via* tautomerism of amide groups (NH-C = O). This feature reveals the mixed presence for the tautomer forms (keto/enol). Surprisingly, molecular modeling using DFT/B3LYP approach verifies the comparable stability of the two forms (keto/enol), implying that their mixed presence produces equivalent probability of their coordination (see part 2.7).

The ^{1}H NMR (DMSO d_6) spectrum of the ligand displayed signals supporting its tautomeric forms as follow; δ 3.82 (s, 2H, CH_2), 6.94–7.81 (m, 8H, Ar-H), 8.12 (d, J = 7.40 Hz, 1H, Ar-H), 10.30 (s, 1H, N(2)H), 10.78 (s, 1H, N(3)H), 11.30 (s, 1H, N(1)H), 12.52 ppm (s, 1H, OH) (Fig. S2). Moreover, the mass spectrum (Fig. S3) of the ligand displayed the molecular ion peak for $[M]^{\cdot+}$ at m/z = 323.24 (0.87 %), which is comparable to its molecular weight and corresponds to $C_{17}H_{14}N_4O_3$ formula. The fragmentation path of the ligand under influence of bombarded electrons was suggested in Scheme 2.

In $[Cu(H_3L)(OAc)_2].H_2O$ complex spectrum, H_3L functions as a neutral tetradentate ligand which coordinates *via* (C = O)$_1$,(C = O)$_2$, (C = O)$_3$ and azomethine nitrogen (C = N)$_{azo}$. The movement of υ(C = O)$_1$, υ(C = O)$_2$, υ(C = O)$_3$ and υ(C = N) to lower wavenumbers aided this coordination mode (Table 2). The fact that υ(NH)$_1$, υ(NH)$_2$ and υ(NH)$_3$ were shifted to higher wavenumbers, suggests that they are no longer coordinated. Furthermore, the novel bands detected at 511 and 459 cm^{-1}can be attributed to υ(Cu-O) and υ(Cu-N), respectively (Nakamoto et al., 1970). The Cu(II) complex has two bands at 1547 and 1344 cm^{-1}, correspond to acetate group vibrations; υ_s(O-C-O) and υ_{as}(O-C-O). The monodentate character of the acetate group was indicated from the difference between those two bands (203 cm^{-1}).

H_3L acts as a mononegative tetradentate within $[UO_2(H_2L)(OAc)]$ and $[Hg(H_2L)(H_2O)Cl]$ complexes. The two carbonyl oxygen [(C = O)$_1$& (C = O)$_2$], the deprotonated enolized carbonyl group (C-O$^-$)$_3$ and the azomethine nitrogen (C = N)$_{azo}$ were the coordinating sites within the two complexes. This chelation mode is based on the simultaneous development of new bands at 1632; 1622 and 1011; 1131 cm^{-1}, which are assigned to υ(C = N*)$_3$ and υ(C-O)$_{enolic(3)}$ (Alharbi et al., 2021), respectively, as well as the disappearance of both υ(C = O)$_3$ and υ(NH)$_3$ vibrations. Also, this mode was supported by the movement of υ(C = O)$_1$, υ(C = O)$_2$ and υ(C = N) vibrations to lower wavenumbers. The vibrations of υ(M−O) and υ(M−N) (Alharbi et al., 2021) were detected at 571; 476 and 530; 467 cm^{-1}, respectively. The UO_2(II) complex spectrum displayed two bands at 1547 and 1457 cm^{-1}, which correspond to υ_s(O-C-O) and υ_{as}(O-C-O) vibrations in acetate groups. The difference between those bands (90 cm^{-1}) denotes the acetate group's bidentate nature (Nakamoto et al., 1970). The lack of (NH)$_3$ and (OH) signals in the ^{1}H NMR spectra of the two diamagnetic complexes (UO_2(II) & Hg(II)) underlines the deprotonation of enolized carbonyl oxygen (=C-O-)$_3$ (i.e., Fig. S2). The ^{1}H NMR spectrum of Hg(II) complex displayed the following signals; δ 3.93 (s, 2H, CH_2), 7.13 (d, J = 8.40 Hz, 2H), 7.34 (t, J = 7.20 Hz, 1H), 7.48–7.752 (m, 4H), 7.97 (d, J = 7.80 Hz, 1H), 8.08 (d, J = 7.80 Hz, 1H), 11.82 (s, 1H, NH) and 11.37 ppm (s, 1H, NH). Two sharp bands at 856–868 and 540–581 cm^{-1}regions are attributed to $\rho_r(H_2O)$ and $\rho_w(H_2O)$ (Nakamoto et al., 1970) vibrations, respectively, for coordinating water molecule in Hg(II) complex. Furthermore, the $[UO_2(H_2L)(OAc)]$ complex's IR spectrum shows three bands at 920, 870, and 268 cm^{-1}, which correspond to υ_3, υ_1 and υ_4 vibrations of dioxouranium ion, respectively. Based on McGlynn et al technique (McGlynn et al., 1961), the υ_3 value was utilized to determine the force constant (F) of υ(U = O) from $(\upsilon_3)^2 = (1307)^2(F_{U\text{-}O})/14.103$. The uranyl complex force constant was then used to calculate the U-O bond length (by Å) using Jones's equation: $R_{U\text{-}O} = 1.08\ (F_{U\text{-}O})^{-1/3} + 1.17$ (McGlynn et al., 1961). The computed $F_{U\text{-}O}$ and $R_{U\text{-}O}$ values are 6.987 mdynes $Å^{-1}$ and 1.735 Å, respectively, which are within the uranyl complexes' normal range. Thus, the neutral tetradentate mode of bonding was recorded with Cu(II) ion while the mononegative tetradentate mode was recorded with UO_2(II) or Hg(II) ion. This may refer to the sizes of Cu(II), Hg(II) and U(VI) ions as 1.57, 1.02 and 0.66 Å, respectively. So, the metals with smaller sizes (Hg(II) and U(VI)) prefer the covalence attachment which happened after the ionization of amide group. Also, the time used for grinding the reactants to synthesize the complexes, effects on the mode of bonding. The long time consumed in grinding to prepare UO_2(II) and Hg(II) complexes leads to high heat that may activate the ionization of the ligand particularly with presence of anions (acetate, chloride) in the reaction medium.

3.3. Magnetism, UV–Vis and ESR spectra

The $[Cu(H_3L)(OAc)_2].H_2O$ complex revealed a magnetic moment value of 2.1B.M., which is consistent with that known for d^9-systems. Also, in tetragonally deformed octahedral shape, its spectrum (Fig. S4) reveals a band at 21,786 cm^{-1} and a broad band at 15479 cm^{-1}, which may assign to $^2B_{1g}\rightarrow{}^2E_g$ and $^2E_g\rightarrow{}^2A_{1g}$ transitions, respectively (Lever et al

Table 2 Some IR spectral bands of H_3L and its new complexes.

Compound	υ(NH)$_1$	υ(NH)$_2$	υ(NH)$_3$	υ(C = O)$_1$	υ(C = O)$_2$	υ(C = O)$_3$	υ(C = N)	υ(C = N*)$_3$	υ(C-O)$_3$	υ(CH$_2$)
H_3L	3200	3303	3259	1742	1686	1662	1613	–	–	3009
$[UO_2(H_2L)(OAc)]$	3229	3303	–	1679	1650	–	1603	1632	1011	2954
$[Hg(H_2L)(H_2O)Cl]$	3190	3324	–	1713	1660	–	1606	1622	1131	3083
$[Cu(H_3L)(OAc)_2].H_2O$	3210	3302	3263	1710	1670	1648	1593	–	–	3018

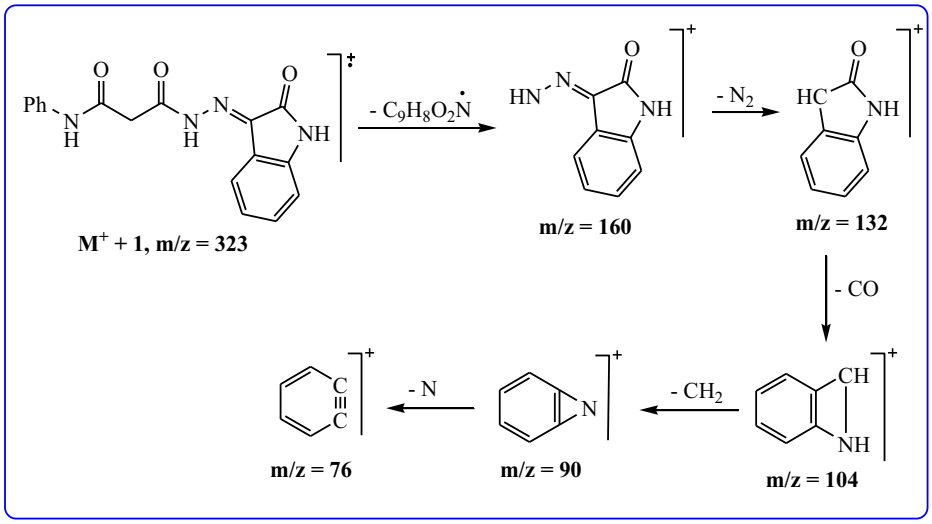

Scheme 2 The pattern of fragmentation for H_3L ligand *3.3. IR, ^{1}HNMR and mass spectra of the complexes.*

1984). The UV–Vis spectrum of $[UO_2(H_2L)(OAc)]$ complex reveals two bands at 29,762 and 23148 cm^{-1}, which attributing to $^1\Sigma_g^+ \rightarrow {}^2\pi_u$ transition in dioxouranium (VI) and n → π* charge transfer, respectively (Al-Fahemi et al 2017).

At room temperature, ESR spectrum of Cu(II) complex at υ = 9.435 GHz (Fig. 1) exhibited axially symmetric g factor with $g_{\|} > g_{\perp} > 2.0023$ which agrees with ^2A_1g ($d^2_{X^2-Y^2}$), as a ground term for octahedral geometry (Abou-Hussen et al., 2005; Hathaway et al., 1984). The G factor could being calculated by using the following expression: $G = (g_{\|} - 2) / (g_{\perp} - 2) = 4$. The factor G as the exchange interaction parameter (Welleman et al., 1978), if it is bigger than 4, the exchange interaction between copper centers in the solid sample is insignificant, according to Hathaway. But, if it < 4, the exchange interaction between copper centers in the solid sample is very significant. The computed value (4.6) indicates that there is no interaction between copper centers in neighboring molecules. Also, the $g_{\|}/A_{\|}$ ratio was 138, which indicates that the deformed octahedral has a critical distortion for dihedral angle in xy-plane. The values 2.28, 2.06, and 165 cm^{-1} were determined as the g-tensor parameters of $g_{\|}$, $g_{\perp}$ and $A_{\|}$, respectively. The degree of covalence of either in plane σ-bonding or in-plane π-bonding between copper ion and the ligand, was estimated by using known equations (Bagdatil et al., 2017). The values of α^2 and β^2 appear to be 0.80 and 0.77, respectively. These values revealed the dominance of ionic property in Cu(II)-L bonds.

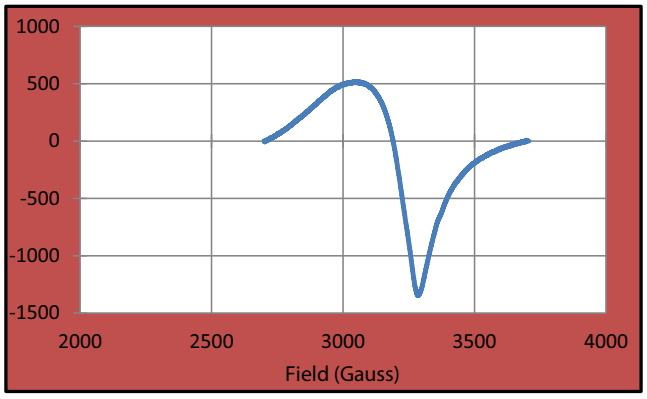

Fig. 1 ESR spectrum of $[Cu(H_3L)(OAc)_2].H_2O$ Complex.

3.4. SEM, XRD and EDX studies

The surface topography of various complexes (Fig. S5) was studied using accelerated beam of electrons in SEM technique (Al-Fahemi et al., 2018). As seen, a regular spherical particles are randomly dispersed between particles produced as frozen rocks in the surface of UO_2(II) and Hg(II) complexes. On the other side, the Cu(II) complex morphology incorporates spherical particles in the form of shattered glacial boulders and micrometer-sized particles.

Cu/Ka derived X-ray diffraction (λ = 1.5406) which directed to investigate the crystal lattice of the Cu(II) complex at 25 °C. The diffraction pattern of the investigated compound (Fig. 2) was extracted in the range of 10° < 2θ < 80°(Khan et al., 2013). Sharp peaks noticed in the model, reveal a well-defined crystal structure formed. The crystal size was calculated using Debye-Scherrier equation [b = 0.94 λ/(S cos θ)] based on FWHM (b) for the characteristic peak. The crystal lattice parameters and particle size had magnitudes of 21.94, 2.062, 0.23, and 530, respectively, corresponding to θ°, d (A°), FWHM (β) and I. The particle size S (nm) was found to be 1.47 nm and based on Bragg equation (nλ = 2d sin θ) at n = 1, the inner crystal plane d-spacing value was calculated (1.945 Å).

Using energy-dispersive x-ray microanalysis (Alkhatib et al 20 20), the complex formation was confirmed, and the elemental mass percentage (wt %) was calculated. An induced radiation (x-ray) was directed towards the solid samples to access inner shells (K- or L-shell) and interact with resident electrons. Following this, the electrons are evacuated and then creating positively charged gaps which can be filled with electrons from L or M shells. K-series (Ka1, Ka2, or Kb) or L-series was created from energy loss according to the shift from upper levels

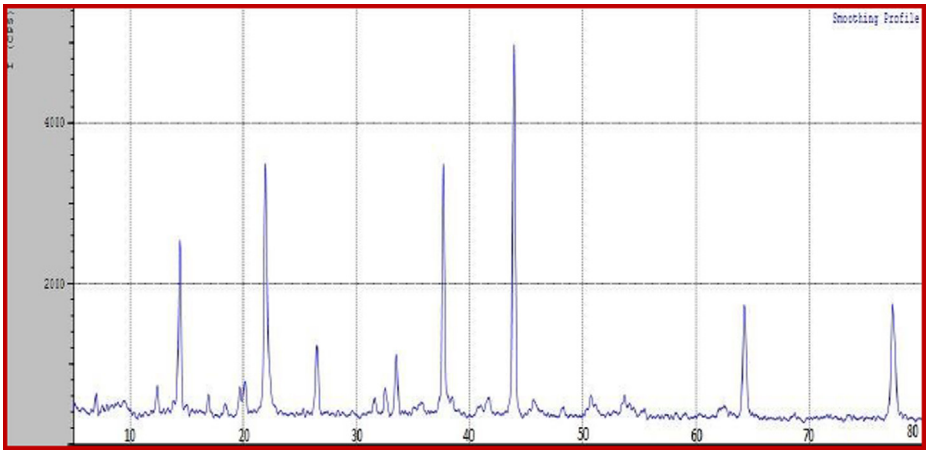

Fig. 2 XRD pattern of $[Cu(H_3L)(OAc)_2].H_2O$ complex.

(L or M) to lower level (Ka1, Ka2, or Kb). The L-series, which is useful in EDX analysis, can be used to get the elemental percentage. Each element's unique electrical structure is represented by a singlet-set of peaks (Fig. 3). The heavier element (metal) was employed to express mass percentage (wt%), while lighter elements (C, H, and O) were not. This identification was carried out over a long time to improve the signals in a variety of locations. The elemental molar ratios computed (wt/At%) matched those obtained from analyses of elements (C, N, O, Cl & M).

3.5. TGA of Cu(II) complex

In the temperature range of 37–125 °C, the TGA curve of $[Cu(H_3L)(OAc)_2].H_2O$ complex (Fig. S6) exhibits 3.44 % weight loss, which corresponds to water of crystallization. The TGA curve shows 23.08 % weight loss between125 and 258 °C, which could assign to the elimination of two acetic acid molecules (Rakha et al., 1989). The TGA curve shows a 17.50% weight loss in the range of 285–430 °C, which may be due to a weakly bonded moiety (C_6H_5N). The residual part ($CuC_{11}H_6O_3N_3$) was recorded at 430 °C with weight percentage of 55.98. Such proposed behavior over the TGA curve, confirms the existence of crystal water molecule and the whole molecular formula of the complex (Table S1). While, the incomplete degradation for the complex indicates the stability of coordination environment surrounds the copper ion.

3.6. Mass spectral analysis

In the lack of chance to isolate x-ray single crystal, the mass spectral analysis has necessity to confirm the molecular formulae of the new complexes which suggested based on former studies (Fig. S7). The signals yielded from fragmentation of the two selected complexes [UO_2(II) and Hg(II)] were obtained over a broad mass range (m/z = 50–1000) under a fixed rate of heating (40 °C/min) and at 70 ev. The molecular ion peaks of UO_2(II) and Hg(II) complexes were appeared at m/z = 651.83 (calcd. 649.34) and m/z = 558.85 (calcd. 574.44). The molecular ion peaks agree perfectly with the molecular weights suggested from elemental analysis but with Hg(II) complex the recorded peak assign to $[(M^+ + 1) - H_2O]$

3.7. Structural verification via computations

The DFT/B3LYP approach was used to improve the structures of the ligand forms (keto/enol) and two of its complexes [Cu(II) & Hg(II)] using Gaussian 09 software (Frisch et al., 2009). All compounds were optimized under 6-31G* basis set except the Hg(II) complex, which was optimized by using the efficient core potential basis set (SDD) level (Lee et al., 1988; Li et al., 2016). The best structural forms (Fig. S8), frontier orbital patterns (Fig. 4), and electrostatic potential (MEP) were extracted from produced files (Fig. S9).

The optimized geometry of H_3L ligand revealed a specific arrangement for C(8) = O(13), C(10) = O(14), N(12) = C(15), and C(16) = O(20) groups, which clarifies their great potential for coordination with metal ions. The charges on coordinating sites in the ligand-keto form were O(13)(-0.397459), O(14)(-0.404351), N(12)(-0.162038), and O(20)(-0.372683) (Al-Qahtani et al., 2021). While, in its enol form, the values were O(13) (-0.412866), O(14) (-0.553187), N(12) (-0.352544), and O(20) (-0.352544). The values in the two forms are near enough to allow for similar coordination opportunities. In the Cu(II) complex, Mulliken charges on the coordinating sites are O(13)(-0.47859), O(14)(-0.376319), N(12)(-0.328716), and O(20)(-0.415370), while in the Hg(II) complex, the charges are O(13)(-0.371977), O(14)(-0.240669), N(12)(-0.272094), and O(20)(-0.238556). Except for N(12) and O(20) atoms in the Cu(II) complex due to M → L charge transfer, the charges were essentially lowered from those in the original keto-form due to their coordination towards the metal ions. In the keto form, the groups C(8) = O(13), C(10) = O(14), N(12) = C(15), and C(16) = O(20) have bond lengths of (1.207883), (1.209620), (1.276331), and (1.228438), respectively. As known, the normal property noticed following the coordination of groups, is the elongation of their bonds which already observed in the two complexes.

Furthermore, the formation energy (E, a.u.), dipole moment (D, Debye), E_{HOMO} (eV), E_{LUMO} (eV), and ΔE (E_{LUMO} -E_{HOMO}, eV) for both tautomer forms were calculated to be −1100.56; 9.294; −0.2198, −0.0981 and −0.123 in the keto form, while, −1100.49, 5.552, −0.2128, −0.1024 and −0.110 in the enol form. The formation energy and the energy gap between frontier orbitals (ΔE) reflect the comparable sta-

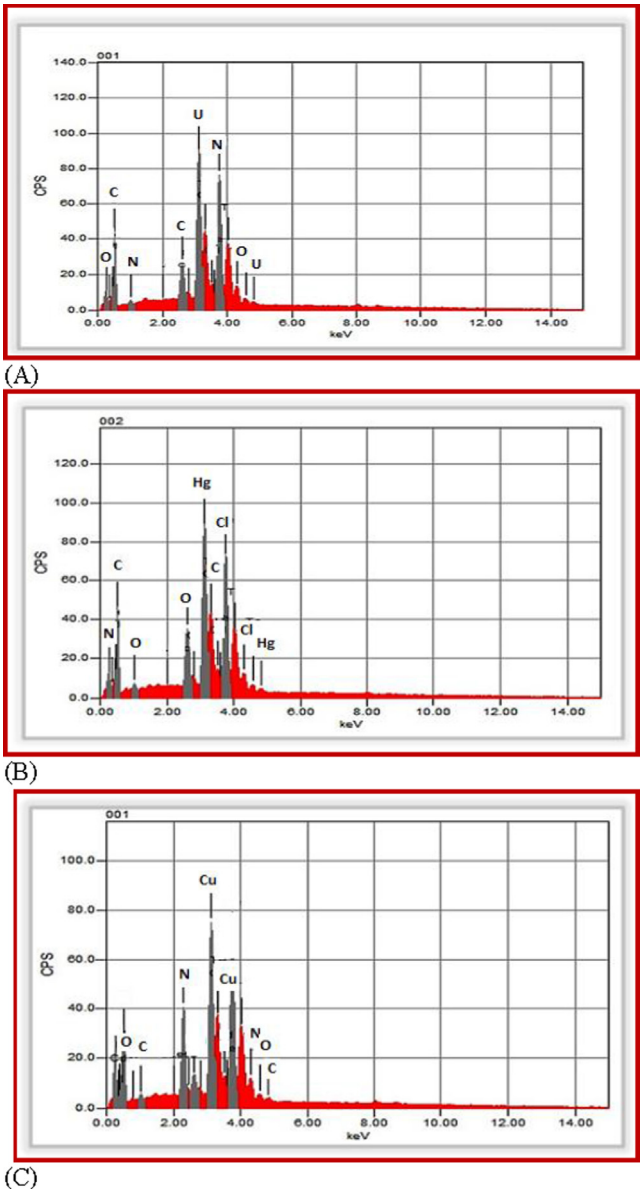

Fig. 3 EDX patterns of(A) UO_2(II), (B) Hg(II) and (C) Cu(II) complexes.

bility of the two forms (Almalki et al 2021). Also, the keto form's large dipole moment aids the coordination, as happened with Cu(II) and Hg(II) ions. Furthermore, these parameters were recovered for the two complexes, with values of −3197.44, 13.21, −0.1695, −0.1402 and −0.029 in the Cu(II) complex and −1790.58, 13.39, −0.1669, −0.1463 and −0.021 in the Hg(II) complex, respectively. The Cu(II) complex's high dipole moment value underlines its high polarity, expects its lower lipophilicity or miscibility in living-cell lipids. As a result, the biological efficiency of the Cu(II) complex may be ineffective, and the Hg(II) complex, regardless of its features, its efficiency in biological filed may be less important.

3.7.1. Characteristics of maps on cubic contours

Establishing new contours to obtain 3D-maps of HOMO and LUMO levels that used to explain the features of electrons distributed on the functional groups (Fig. 3). In terms of the ligand tautomer-forms, the two orbitals largely covered the coordinating centers as O(13), O(14), N(12), and O(20). This measures the fluency of electronic transitions within the coordinating functional groups. The lower ΔE values of −0.123 and −0.110 eV in the keto - enol forms, respectively, corroborated this property (Shaker et al., 2021). Additionally, in Cu (II) or Hg(II) complex, these two orbitals appeared spread over the entire molecule (Fig. 4), indicating that the central atom has an impact on the electronic distribution inside the compound.

In particular, to identify essential features, the molecular electrostatic map (MEP) was generated on the molecular surface (Fig. S9). This map distinguishes the zones of nucleophilic, electrophilic, and neutral in the tautomers of the ligand. So, the nucleophilic behavior of the functional groups towards the metal ions can be assessed to confirm the binding mode within the complexes. The colors red, blue, and green, respectively, appeared on the maps to represent these three zones. In the keto form, the electrostatic potential range was −4.114e-2 to 6.914e-2, while in the enol form, it was −4.413e-2 to 6.413e-2. The red zone was also concentrated on the majority of coordinating centers [O(13), O(14), and O (20)] in the two forms. Whereas, in the Cu(II) or Hg(II) complex, this nucleophilic property was improved due to the inclusion of a secondary ligand (acetate or H_2O) which rises the nucleophilicity of the molecule commonly.

3.8. Cyclic voltammetry

The equations used for this study were presented in the supporting materials (part S1), to minimize the similarity percentage in the document.

3.8.1. Cyclic voltammetry of copper chloride

3.8.1.1. Redox mechanism and effect of different Cu(II) concentrations without H_3L at 298.15 K. As shown in Fig. S10, the redox mechanism of $CuCl_2$ in 0.1 M KCl as a supporting electrolyte and glassy carbon (GC) as a working electrode was investigated using cyclic voltammetry within the potential window of 0.8 to −0.8 V and scan rate of 0.1 V/sec at 298.15 K. The emergence of two cathodic and two anodic peaks correspond to (Cu^{2+}/Cu^{1+}) and (Cu^{1+}/Cu^{0}) on the voltammogram indicates that the Cu(II) solution is electroactive. The two cathodic potential peaks of Cu^{2+}/Cu^{1+} (E_{pc1}) and Cu^{1+}/Cu^{0} (E_{pc2}), were appeared at 0.101 V and −0.322 V in the forward scan, respectively. While, the two anodic potential peaks of Cu^{0}/Cu^{1+}(E_{pa2}) and Cu^{1+}/Cu^{2+}(E_{pa1})were appeared at 0.035 V and 0.212 V in the reverse scan, respectively. As a result, the reaction's redox mechanism can be expressed as follows:

Reduction:	
$Cu^{2+} + e^-$	Cu^{1+} at 0.101 V (1)
$Cu^{1+} + e^-$	Cu at −0.322 V (2)
Oxidation:	
Cu	$Cu^{1+} + e^-$ at 0.035 V (3)
Cu^{1+}	$Cu^{2+} + e^-$ at 0.212 V (4)

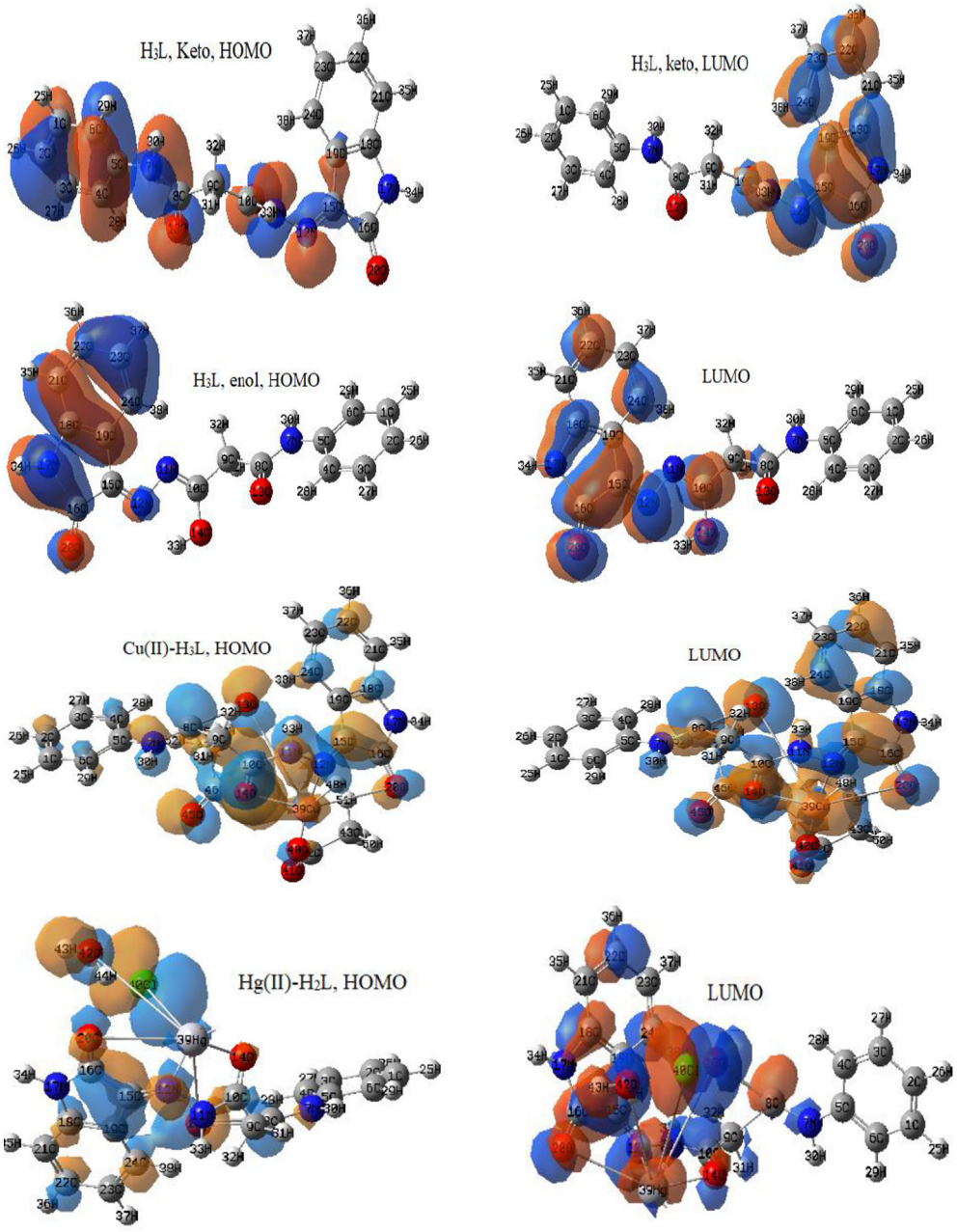

Fig. 4 the patterns of HOMO and LUMO levels in the optimized structures.

Tables S2 and S3 show the estimated and collected thermodynamic parameters for both anodic and cathodic peaks (A and B). With increasing $CuCl_2$ concentration, the majority of the examined parameters I_p, Γ, E° and Q for anodic and cathodic peaks were elevated. The existence of the diffusion process is shown by the increase in all peak currents (Shaikh et al., 2006).

3.8.1.2. Cyclic voltammetry response of Cu(II) in presence of H_3L at 298.15 K. As shown in Fig. S11, we investigated the electrochemical behavior of the complexation between H_3L and $CuCl_2$ in 0.1 M KCl solution within the + 0.8 to −0.8 V potential range. By increasing the ligand concentration and favoring the covalence between the copper ions and H_3L, all of the current peaks for the generated redox peak are reduced. The peak potentials for both cathodic and anodic peaks have also been altered. These outputs assumed that the copper and H_3L have a strong affinity to form a stable complex. Additionally, Tables 3 and S4 summarize the values of peak potential of cathodic (E_{Pc}) and anodic (E_{Pa}), anodic peak potential separation (ΔE_p), peak currents (i_{Pa}, i_{Pc}), peak current ratio (i_{Pa}/i_{Pc}), standard potential (E), standard heterogeneous electron transfer rate constant (k_s), charge transfer coefficient (α_{na}), surface coverage (Γ), and the quantity of charge (Q) for $CuCl_2$ that obtained from previous voltammogram under influence of H_3L in different concentrations.

3.8.1.3. Effect of scan rates on Cu(II) in absence or presence of H_3L at 298.15 K. Figs. S11 and 5 show cyclic voltammograms

Table 3 The parameters of Kinetic and Thermodynamic for $CuCl_2$ wave (A) in presence of H_3L and at 298.15 K and 0.1 scan rate.

Mx10^6 (mol/cm^3)	Lx10^6 (mol/cm^3)	Epa (volt)	Epc (volt)	ΔEp (volt)	-Ipa x10^5 (Amp)	Ipc x10^5 (Amp)	Ip,a/ Ipc (Amp)	E˙	Da x10^6 (cm^2/s)	Dc x10^6 (cm^2/s)	αn_a	Ks x10^2 (cm/sec)	Γc x10^9 (mol/cm^2)	+ Qc x10^5	Γa x10^9 (mol/cm^2)	- Qa x10^5
3.21	0.64	0.194	0.078	0.116	1.66	3.35	0.494	0.136	3.75	0.15	0.782	4.60	11.37	3.45	5.615	1.70
3.18	1.27	0.209	0.067	0.142	1.47	3.22	0.456	0.138	2.98	0.14	0.648	5.23	10.91	3.31	4.978	1.51
3.16	1.90	0.251	0.073	0.178	1.27	2.72	0.468	0.162	2.28	0.10	0.613	6.12	9.222	2.79	4.320	1.31
3.14	2.52	0.250	0.083	0.166	1.26	2.91	0.434	0.166	2.27	0.12	0.650	6.07	9.872	2.99	4.287	1.30
3.13	3.13	0.286	0.091	0.195	0.82	1.66	0.494	0.189	0.97	3.98	0.764	5.00	5.643	1.71	2.787	0.84
3.08	4.62	0.333	0.099	0.235	0.89	1.28	0.701	0.216	1.19	2.42	0.708	5.52	4.331	1.31	3.034	0.92
3.03	6.06	0.328	0.121	0.207	0.97	1.02	0.956	0.224	1.44	1.58	0.738	3.49	3.445	1.04	3.293	0.99
2.94	8.82	0.329	0.134	0.329	1.19	0.85	1.398	0.164	2.30	1.18	0.234	5.60	2.889	0.88	4.040	1.22

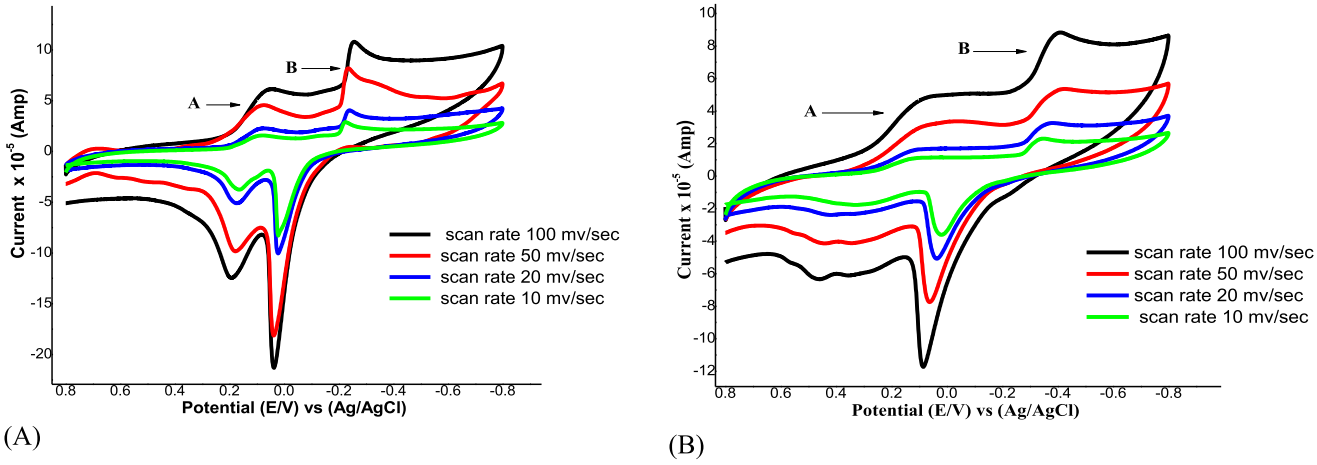

Fig. 5 Cyclic voltammograms of $CuCl_2$ at different scan rates in absence (A) and in presence (B) of H_3L and at 298.15 K.

of Cu(II) in absence or presence of H_3L at 298.15 K in 0.1 M KCl and at various scan rates of 10, 20, 50, and 100 mV/s. It has been discovered that, (i) increasing the scan rate, either cathodic or anodic peak currents rise in a linear manner. (ii) As the scan rate increased, the cathodic peak changed slightly towards the negative potential and the anodic peak shifted slightly towards the positive potential. The linear relationship between the square root of scan rate and peak currents, as seen in Figs. S12 and 6, supports the idea of diffusion-controlled redox process. The ratio of current peak is > 1, implying that the system is quasi-reversible (Zaky et al 2012). The solvation and kinetic characteristics for the cathodic and anodic of $CuCl_2$ in the absence or presence of H_3L at different scan rates are explained in Tables S5, S6, 4 and 5.

3.8.1.4. Gibbs free energies and the stability constant of Cu- H_3L complex at 298.15 K. By raising the ratio (j) and ligand concentration, the Gibbs free energies (ΔG) and stability constants (log β_{MX}) for the copper ions that reacted with H_3L to form complex are raised. This indicating greater complexation was occurred as shown in Tables S7 and S8. By adjusting the scan rate, we were able to see how the stability constant changed. As seen in Tables S9 and S10, when the scan rate is reduced, the complex's stability constant increases, indicating a diffusion-controlled response.

3.9. Biological investigation

3.9.1. Effect of compounds toward E. Coli, S. Aureus and C. Albicans

Based on the width of the inhibition zone (Table 6), the majority of the isolated compounds have modest antibacterial activ-

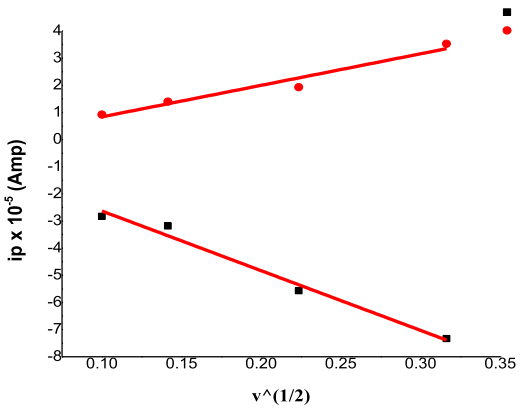

Fig. 6 Relation (i_p *vs.* $v^{1/2}$) for $CuCl_2$ in presence of H_3L by the molar ratio (1:1) and different scan rates.

Table 4 Effect of different scan rates on $CuCl_2$ [3.23x10^{-6} M] in absence of H_3L at 298.15 K for wave (B).

υ (V/sec)	Epa (volt)	Epc (volt)	ΔEp (volt)	-Ipa x10^5 (Amp)	Ipc x10^5 (Amp)	Ipa/Ipc (Amp)	E°	Da x10^5 (cm^2/s)	Dcx10^5 (cm^2/s)	αn$_a$	Ks x10^2 (cm/sec)	Γc x10^8 (mol/cm^2)	+ Qc x10^5	Γa x10^8 (mol/cm^2)	- Qa x10^5
0.1	0.037	−0.256	0.292	17.7	4.01	4.411	−0.109	4.24	2.177	2.169	0.51	1.362	4.13	6.007	18.2
0.05	0.035	−0.236	0.267	18.1	3.54	5.117	−0.098	8.86	3.383	3.407	0.44	2.401	7.27	12.29	37.2
0.02	0.023	−0.232	0.213	9.26	1.51	6.151	−0.129	5.79	1.530	3.66	0.12	2.554	7.74	15.70	47.6
0.01	0.021	−0.223	0.244	7.81	1.16	6.711	−0.101	8.24	1.829	3.976	0.13	3.948	12.0	26.50	80.3

Table 5 Effect of different scan rates on Cu- H_3L complex for wave (B) and at 298.15 K.

υ (V/sec)	Epa (volt)	Epc (volt)	ΔEp (volt)	-Ipa x10^5 (Amp)	Ipc x10^5 (Amp)	Ipa/Ipc (Amp)	E°	Da x10^5 (cm^2/s)	Dcx10^5 (cm^2/s)	αn$_a$	Ks x10^2 (cm/sec)	Γc x10^8 (mol/cm^2)	+ Qc x10^5	Γa x10^8 (mol/cm^2)	- Qa x10^5
0.1	0.084	−0.339	0.423	7.33	3.53	2.080	−0.128	7.738	1.789	7.951	3.15	1.196	3.62	2.488	7.54
0.05	0.059	−0.394	0.453	5.57	1.93	2.878	−0.168	8.916	1.076	0.722	0.70	1.312	3.97	3.776	11.4
0.02	0.032	−0.367	0.399	3.18	1.40	2.278	−0.168	7.273	1.402	0.823	0.32	2.367	7.17	5.392	16.3
0.01	0.012	−0.339	0.351	2.83	0.92	3.072	−0.164	11.49	1.217	1.192	0.16	3.120	9.45	9.584	29.0

Table 6 The antimicrobial activity of H_3L and its complexes.

Compound	*E. coli* (mg/ml)		*S. aureus* (mg/ml)		*C. Albicans* (mg/ml)	
	Diameter of inhibition zone (in mm)	% Activity index	Diameter of inhibition zone (in mm)	% Activity index	Diameter of inhibition zone (in mm)	% Activity index
H_3L	7	29	9	41	4	14
$[UO_2(H_2L)(OAC)]$	12	53	10	49	11	34
$[Cu(H_3L)(OAC)_2].H_2O$	6	22	7	28	9	30
$[Hg(H_2L)(H_2O)Cl]$	18	69	15	64	14	45
Ampicillin	24	100	22	100	NA	NA
Colitrimazole	NA	NA	NA	NA	28	100

ity against all organisms. The Hg(II) complex exhibits the strongest antibacterial activity against *Escherichia coli* (69%) followed by UO_2(II) complex (53%) and Cu(II) complex (22 %). The antifungal activity of Hg(II) Complex is the strongest, followed by UO_2(II) Complex. Although, the toxic effect of Hg (II) ion was greatly reduced due to its coordination, but its biological uses are limited till now, just used in treatment for some skin diseases.

3.9.2. Antioxidant activity for ABTS method

The antioxidant activity of all investigated compounds was determined using ABTS assay (Aljohani et al., 2021). According to the data, all complexes exhibited lower antioxidant activity than the ligand (21.91%), except the UO_2(II) complex (28.72%), which reveals a significant antioxidant activity when compared to conventional ascorbic acid (Table S11). The presence of two carbonyl oxygen $(C = O)_1$, $(C = O)_2$, azomethine nitrogen $(C = N)_{azo}$, hydroxyl group (OH) and two NH groups in H_3L resulted in substantial antioxidant activity which may be banned due to incomprehensible mechanics. This did not motivate us to investigate their antioxidant behavior by another methods.

3.9.3. Cell proliferation assay

We were able to examine the ability of the ligand and its complexes to suppress cancer cell proliferation in Hepatocellular carcinoma liver (HCC) due to the biological activity of Schiff bases (Singh et al., 2017; Konakanchi et al., 2018). IC_{50} values

Table 7 Cytotoxicity (IC_{50}) of H_3L and its metal complexes on HepG2 cell line.

Compound	IC_{50}(μg/ml)
5-FU	2.60
H_3L	5.60
$[UO_2(H_2L)(OAC)]$	4.51
$[Cu(H_3L)(OAC)_2].H_2O$	6.71
$[Hg(H_2L)(H_2O)Cl]$	10.80

(compound concentrations that cause 50% cell death) were calculated in our experiments. Under the same experimental circumstances, the cytotoxicity of Fluorouracil (5-FU), the free ligand, and metal complexes was assessed for comparison. The presence of metal ions shows a synergistic effect on the cytotoxicity (Table 7). The results reveal that the IC_{50} values are substantially lower in the UO_2(II) complex (4.51 μg/ml) than in the ligand (5.60 μg/ml) alone. These values reflect the effective anticancer activity of the UO_2(II) complex and the free ligand. The Hg(II) complex, on the other hand its IC_{50} value (10.80 μg/ml), reflects its moderate anticancer activity towards the liver carcinoma cell line (Mandal et al., 2018; Mallela et al., 2018).

4. Conclusion

Cu(II), Hg(II) and UO_2(II) ions were coordinated with (*E*)-3-oxo-*N'*-(2-oxoindolin-3ylidene)-3-(phenylamino)propane hydrazide through solvent free synthesis way. These new compounds were deliberately identified by utilizing all available techniques that covering analytical and spectral types. A distorted octahedral arrangement around the central atom, was suggested for the three complexes. The mode of bonding within the Cu(II) and Hg(II) complexes was confirmed by DFT method through Gaussian 09 under 6-31G* and SDD basis sets. In addition, cyclic voltammograms were performed for Cu(II) ion under different conditions to estimate solvation and kinetic characteristics as well as to throw a shadow on the impact of complex formation on the electrochemical manners. Both of the ligand and copper ion displayed high affinity towards the coordination in solution which coincides with that in solid state. On the other side, the antimicrobial, antioxidant and antitumor activity of the prepared compounds were examined *in-vitro* and the activity is generally in moderate to low significance. A notable cytotoxicity was appeared with UO_2(II) complex and the ligand.

Acknowledgments

Taif University Researchers Supporting Project number (TURSP-2020/23). Taif University, Taif, Saudi Arabia.

Data availability

All relevant data are within the manuscript and available from the corresponding author upon request.

Appendix A. Supplementary data

Supplementary data to this article can be found online at https://doi.org/10.1016/j.arabjc.2021.103586.

References

Abou-Hussen, A.A., El-Metwaly, N.M., Saad, E.M., El-Asmy, A.A., 2005. Spectral, magnetic, thermal and electrochemical studies on phthaloyl bis(thiosemicarbazide) complexes. J. Coord. Chem. 58, 1735–1749.

Abu-Dief, A.M., El-khatib, R.M., Aljohani, F.S., Alzahrani, S.O., Mahran, A., Khalifa, M.E., El-Metwaly, N.M., 2021. Synthesis and intensive characterization for novel Zn (II), Pd (II), Cr (III) and VO (II)-Schiff base complexes; DNA-interaction, DFT, drug-likeness and molecular docking studies. J. Mol. Struct. 130693. https://doi.org/10.1016/j.molstruc.2021.130693.

Abumelha, H.M., Al-Fahemi, J.H., Althagafi, I., Bayazeed, A.A., Al-Ahmed, Z.A., Khedr, A.M., El-Metwaly, N.M., 2020. Deliberate-characterization for Ni (II)-Schiff base complexes: promising in-vitro anticancer feature that matched MOE docking-approach. J. Inorg. Organomet Polym., 1–17

Al-Fahemi, J., Saad, H.F.A., El-Metwaly, N.M., Farghaly, T.A., Elghalban, M.G.K., Saleh, A., Al-Hazmi, G., 2017. A Synthesis of Co (II), Cu (II), Hg (II), UO2 (II) and Pb (II) binuclear nanometric complexes from multi-donor ligand: Spectral, modeling, quantitative structure–activity relationship, docking and antitumor studies. Appl. Organomet. Chem. 31, (11) e3787.

Al-Fahemi, J.H., Khedr, A.M., Althagafi, I., El-Metwaly, N.M., Saad, F.A., Katouah, H.A., 2018. Green synthesis approach for novel benzenesulfonamide nanometer complexes with elaborated spectral, theoretical and biological treatments. Appl. Organomet. Chem. 32, 4460.

Alharbi, A., Alzahrani, S., Alkhatib, F., Abu Al-Ola, K., Abdulaziz, A.A., Zaky, R., El-Metwaly, N.M., 2021. Studies on new Schiff base complexes synthesized from d10 metal ions: Spectral, conductometric measurements, DFT and docking simulation. J. Mol. Liq. 334, 116–148.

Al-Hazmi, G.A.A., El-Metwally, N.M., 2017. A series of nickel(II) complexes derived from hydrazide derivatives, electrochemical, thermal and spectral studies. Arab. J. Chem. 10, S1003–S1013. https://doi.org/10.1016/j.arabjc.2013.01.002.

Aljohani, F.S., Abu-Dief, A.M., El-Khatib, R.M., Al-Abdulkarim, H. A., Alharbi, A., Mahran, A., Khalifa, M.E., El-Metwaly, N.M., 2021. Structural inspection for novel Pd (II), VO (II), Zn (II) and Cr (III)-azomethine metal chelates: DNA interaction, biological screening and theoretical treatments. J. Mol. Strut. 1246, 131139.

Alkhatib, F., Hameed, A., Sayqal, A., Bayazeed, A.A., Alzahrani, S., Al-Ahmed, Z.A., Zaky, R., El-Metwaly, N.M., 2020. Green-synthesis and characterization for new Schiff-base complexes; spectroscopy, conductometry, Hirshfeld properties and biological assay enhanced by in-silico study. Arab. J. Chem. 13, 6327–6340. https://doi.org/10.1016/j.arabjc.2020.05.033.

Almalki, S.A., Bawazeer, T.M., Asghar, B., Alharbi, A., Aljohani, M. M., Khalifa, M.E., El-Metwaly, N.M., 2021. Synthesis and characterization of new thiazole-based Co (II) and Cu (II) complexes; therapeutic function of thiazole towards COVID-19 in comparing to current antivirals in treatment protocol. J. Mol. Struct. 1244, 130961.

Al-Qahtani, S.D., Alsoliemy, A., Almehmadi, S.J., Alkhamis, K., Alrefaei, A.F., Zaky, R., El-Metwaly, N.M., 2021. Green synthesis for new Co (II), Ni (II), Cu (II) and Cd (II) hydrazone-based complexes; characterization, biological activity and electrical conductance of nano-sized copper sulphate. J. Mol. Struct. 1244, 131238.

Alzahrani, S., Morad, M., Bayazeed, A., Aljohani, M., Alkhatib, F., Shah, R., Katouah, H., Abumelha, H.M., Althagafi, I., Zaky, R., El-Metwaly, N.M., 2020. Ball milling approach to prepare new Cd (II) and Zn (II) complexes; characterization, crystal packing, cyclic voltammetry and MOE-docking agrees with biological assay, J. Mol. Struct 1218, 28473. https://doi.10.1016/j.molstruc.2020.128473.;

Atkins, A.J., Black, D., Blake, A.J., Marin-Bocerra, A., Parsons, S., Ruiz-Ramirez, L., Schröder, M., 1996. Chem. Commun. 4, 457

Bagdatil, E., Altuntas, E., Sayin, U., 2017. Synthesis and structural characterization of new oxovanadium (IV) complexes derived from azo-5-pyrazoleone with prospective medical importance. J. Mol. Struct. 1127, 653–661.

Becke, A.D., 1993. Density-functional thermochemistry III. The role of exact exchange. J. Chem. Phys. 98 (7), 5648–5652.

Dennington, R., Keith, T., Millam, J., 2007. Gauss View, Version 4.1.2, Semichem Inc., Shawnee Mission, KS.

Fisher, B.J., Eisenberg, R., 1980. Electrocatalytic reduction of carbon dioxide by using macrocycles of nickel and cobalt. J. Am. Chem. Soc. 102, 7361–7363. https://doi.org/10.1021/ja00544a035

Frisch, M., Trucks, G., Schlegel, H., Znseria, G.S., Robb, M., Cheeseman, J., Scalmani, G., Barone, V., Mennucci, B., Petersson, G., 2009. Gaussian 09 Revision A. 1, Wallingford, CT, USA.

Geary, W.J., 1971. The use of conductivity measurements in organic solvents for the characterisation of coordination compounds. Coord. Chem. Rev. 7, 81–122.

Hathaway, B.J., 1984. A new look at the stereochemistry and electronic properties of complexes of the copper(II) ion. Struct. Bonding (Berlin) 57, 55–118.

Hawkey, P.M., Lewis, D.A., 1994. Medical bacteriology – a practical approach. Oxford University Press, United Kingdom, p. 181.

Katouah, H.A., Al-Fahemi, J.H., Elghalban, M.G., Saad, F.A., Althagafi, I.A., El-Metwaly, N.M., Khedr, A.M., 2019. Synthesis of new Cu (II)-benzohydrazide nanometer complexes, spectral, modeling, CT-DNA binding with potential anti-inflammatory and anti-allergic theoretical features. Mater. Sci. Eng. C96, 740-756. https://doi.10.1016/j.msec.2018.11.034

Katouah, H., Hameed, A.M., Alharbi, A., Alkhatib, F., Shah, R., Alzahrani, S., Zaky, R., El-Metwaly, N.M., 2020a. Green Synthesis Strategy for New Schiff-Base Complexes: Characterization, Conductometry, In Vitro Assay Confirmed by In Silico Approach. ChemistrySelect. 5 (33), 10256–10268. https://doi.org/10.1002/slct.202002388.

Katouah, H., Sayqal, A., Al-Solimy, A.M., Abumelha, H.M., Shah, R., Alkhatib, F., Alzahrani, S., Zaky, R., El-Metwaly, N.M., 2020b. Facile synthesis and deliberate characterization for new hydrazide complexes; cyclic voltammetry, crystal packing, eukaryotic DNA degradation and in-silico studies. J. Mol. Liq. 320, e114380.

Khan, M.I., Khan, A., Hussain, I., Khan, M.A., Gul, S., Iqbal, M., Khuda, F., 2013. Spectral, XRD, SEM and biological properties of new mononuclear Schiff base transition metal complexes. Inorg. Chem. Commun. 35, 104–109.

Konakanchi, R., Haribabu, J., Nishtala, J.V.B., Mallela, R., Manchala, S., Gandamalla, D., Karvembu, R., Reddy, B.V., Yellu, N. R., Kotha, L.R., 2018. Synthesis, Structural, Biological Evaluation, Molecular Docking and DFT Studies of Co(II), Ni(II), Cu(II), Zn (II), Cd(II) and Hg(II) Complexes bearing Heterocyclic Thiosemicarbazone ligand. Appl. Organomet. Chem. e4415.

Lee, C., Yang, W., Parr, R.G., 1988. Development of the Colle-Salvetti correlation-energy formula into a functional of the electron density. Phys. Rev. B 37 (2), 785–789.

Lever, A.B.P., 1984. Inorganic Electronic Spectroscopy. Elsevier, New York.

Li, L., Hu, J., Shi, X., Ruan, W., Luo, J., Wei, X., 2016. Theoretical Studies on Structures, Properties and Dominant Debromination Pathways for Selected Polybrominated Diphenyl Ethers. Int. J. Mol. Sci. 17 (6), 927.

Munshi, M.A., Bayazeed, A.A., Abualnaja, M., Morad, M., Alzahrani, S., Alkhatib, F., Shah, R., Zaky, R., El-Metwaly, N.M., 2021. Ball-milling synthesis technique for Cu (II)-Schiff base complexes with variable anions; characterization, potentiometric study and in-vitro assay confirmed by in-silico method. Inorg. Chem. Commun., 127, 108542. https://doi.10.1016/j.inoche.2021.108542.n

Mallela, R., Konakanchi, R., Nethaji, R.G., Yellu, M.D.G.N.R., Kotha, L.R., 2018. Zn(II), Cd(II) and Hg(II) metal complexes of 2-aminonicotinaldehyde: Synthesis, crystal structure, biological evaluation and molecular docking study. Inorganica. Chim. Acta. 469, 66–75.

Mandal, S., Mondal, M., Biswas, J.K., Cordes, D.B., Slawin, A.M.Z., Butcher, R.J., Saha, M., Saha, N.C., 2018. Synthesis, characterization and antimicrobial activity of some nickel, cadmium and mercury complexes of 5-methyl pyrazole-3yl-N-(2′-methylthiophenyl) methyleneimine, (MPzOATA) ligand. J. Mol. Struct. 1152, 189–198.

McGlynn, S.P., Smith, J.K., 1961. Electronic Structure, Spectra, and Magnetic Properties of Oxycations. III. Ligation Effects on the Infrared Spectrum of the Uranyl Ion. J. Chem. Phys. 35, 105.

Mohamed, S.M., Kotb, E.R., Abd El-Meguid, E.A., Awad, H.M., 2017. Synthesis and solid-state fluorescence of 2-alkylamino-4-aminopyridine-3,5-dicarbonitriles. Res. Chem. Intermed. 43, 437.

Morgan, Sh.M., El-Sonbati, A.Z., Eissa, H.R., 2017. Geometrical structures, thermal properties and spectroscopic studies of Schiff base complexes: Correlation between ionic radius of metal complexes and DNA binding. J. Mol. Liq. 240, 752–776.

Mosmann, T., 1983. Rapid Colorimetric Assay for Cellular Growth and Survival: Application to Proliferation and Cytotoxicity Assays. J. Immunol. Methods 65, 55.

Nakamoto, K., 1970. Infrared spectra of inorganic, coordination compounds. Wiley Interscience, New York.

Antony, R., David, S.T., Saravanan, K., Karuppasamy, K., Balakumar, S., 2013. Synthesis, spectrochemical characterisation and catalytic activity of transition metal complexes derived from Schiff base modified chitosan. Spectrochim. Acta A. 103, 423.

Rakha, T.H., Ibrahim, K.M., Khalifa, M.I., 1989. Thermochemical study of some transition metal complexes of isonicotinic hydrazide derivatives. Thermochim. Acta. 144, 53–63. https://doi.org/10.1016/0040-6031(89)85084-1.

Re, R., Pellegrini, N., Proteggente, A., Pannala, A., Yang, M., Rice-Evans, C., 1999. Antioxidant activity applying an improved ABTS radical cation decolorization assay. Free Radic. Biol. Med. 26, 1231–1237.

Shah, R., Katouah, H., Sedayo, A.A., Abualnaja, M., Aljohani, M. M., Saad, F., Zaky, R., El-Metwaly, N.M., 2020. Practical and computational studies on novel Schiff base complexes derived from green synthesis approach: conductometry as well as in-vitro screening supported by in-silico study. J. Mol. Liq. 319,. https://doi.org/10.1016/j.molliq.2020.114116 114116.

Shaikh, A.A., Begum, M., Khan, A.H., Ehsan, M.Q., 2006. Cyclic voltammetric studies of the redox behavior of iron (III)-vitamin B6 complex at carbon paste electrode. Russ. J. Electrochem. 42, 620.

Shaker, M., Adam, S., Shaaban, S., Khalifa, M.E., Alhasani, M., El-Metwaly, N.M., 2021. New Cu (II) and VO (II)-O, N, O-aroylhydrazone complexes: Biological evaluation, catalytic performance, ctDNA interaction, DFT, pharmacophore, and docking simulation. J. Mol. Liq. 335, 116554.

Singh, M.K., Sutradhar, S., Paul, B., Adhikari, S., Laskar, F., Butcher, R.J., Acharya, S., Das, A., 2017. A new cadmium(II) complex with bridging dithiolate ligand: Synthesis, crystal structure and antifungal activity study. J. Mol. Struct. 1139, 395–399.

Sönmez, M., Celebi, M., Berber, I., 2010. Synthesis, spectroscopic and biological studies on the new symmetric Schiff base derived from 2,6-diformyl-4-methylphenol with N-aminopyrimidine. Eur. J. Med. Chem. 45, 1935–1940. https://doi.org/10.1016/j.ejmech.2010.01.035.

Tamami, B., Ghasemi, S., 2015. Catalytic activity of Schiff-base transition metal complexes supported on crosslinked polyacrylamides for hydrogen peroxide decomposition. J. Organomet, Chem. 794, 311–317. https://doi.org/10.1016/j.jorganchem.2015.05.041.

Vogel, A.I., 1989. Quantitative Inorganic Analysis. Longmans, London.

Welleman, J.A., Hulsbergen, F.B., 1978. Influence of alkyl chain length in N-alkyl imidazoles upon the complex formation with transition-metal salts. J. Inorg. Nucl. Chem. 40, 143–147.

Zaky, R.R., Yousef, T.A., Ibrahim, K.M., 2012. Co(II), Cd(II), Hg(II) and U(VI)O_2 complexes of o-hydroxyacetophenone [N-(3-hydroxy-2-naphthoyl)] hydrazone: Physicochemical study, thermal studies and antimicrobial activity. Spectrochim. Acta A 97, 683–694.